Large-Scale Experiment and Numerical Modeling of Riverine Levee Breach

Takaharu Kakinuma[1] and Yasuyuki Shimizu[2]

Abstract: This study aims to clarify the mechanism of riverine levee breach and propose a new numerical model for that phenomenon. We performed large-scale experiments of overtopping breach using an experimental flume located on the floodway of an actual river channel. By taking advantage of the scale of the flume, we monitored the levee breach process with state-of-the-art observation devices under highly precise hydraulic conditions. We performed four test cases with variations of inflow rate, levee material and levee shape, and monitored the levee breach quantitatively using acceleration sensors installed in the levee body. From the results of the experiments, we categorized the breach process into four stages, focusing on the breach progress and hydraulic characteristics. We determined that the correlation between the breached volume and the hydraulic quantities of velocity, water level and Shields number can be expressed by an equation similar to that for bed load transport. Finally, we proposed a two-dimensional numerical model by integrating the experimental results into geomechanics, and we obtained a fine reproduction result.

[1] Deputy Team Leader, River Engineering Research Team, Civil Engineering Research Institute for Cold Region, Japan.

[2] Professor, Laboratory of Hydraulic Research, Graduate School of Engineering, Hokkaido University, Japan.

Introduction

Recent years have seen a considerably increased incidence of typhoons, torrential rainstorms and other extreme meteorological phenomena due to climate change, thereby raising the risk of large-scale disasters caused by riverine floods. The flood damage is particularly severe when levee breaches occur, so estimating the flood magnitude and providing hazard maps are crucial for risk management. In light of this, we identified an urgent need to clarify the mechanism of riverine levee breach. Most of the riverine levees are earthen embankments, and a variety of research on earthen embankment breaches has been done for decades. That research can be classified as field case studies, laboratory experiments and breach models.

Firstly, field case studies: These are among the most important ways of studying embankment breaches; however, despite considerable effort, only a limited number of real-life, real-time breach events have been investigated because of observation difficulties and safety concerns.

Next, laboratory experiments: Wahl (2007) reviewed a large number of laboratory embankment breach experiments performed over the course of several decades. Most of these experiments were found to be small-scale, except for a few experiments such as the European IMPACT project (Morris and Hassan 2005), the USDA-ARS project (Hanson et al. 2005; Hunt et al. 2005) and Sattar et al. (2008) who performed a mobile bed experiment of the 17th street canal breach by hurricane Katrina and stated the bed of breach was variable. Embankment breach, which depends on interaction among flows, sediment transport and corresponding morphological changes, is so complex that laboratory experiments, especially small-scale ones, encounter scale effects and simplifications that make it difficult to understand the breach processes and to collect reliable data toward developing embankment breach models. Wahl's review also clarified that most of the experiments, including the aforementioned two projects, addressed dam embankment breaches, whereas very few experiments addressed riverine levee breaches.

48 Thirdly, breach models: Many models have been proposed, and the ASCE/EWRI Task Committee on
49 Dam/Levee Breaching (2012) reviewed such models and classified them as parametric models,
50 simplified physically based models or detailed physically based models. According to the review, most
51 of these models addressed overtopping dam breaches, and only a few models addressed riverine levee
52 breaches.

53 Here we attempt to clarify the different characteristics of the dam embankment breaches and riverine
54 levee breaches. Morphologically, the dam breaches are characterized by vertical progress, in contrast to
55 the horizontal advancement of riverine levee breaches. Hydraulically, an overflow direction
56 perpendicular to the cross section characterizes dam breaches, in contrast to oblique overflow for
57 riverine levee breaches. Moreover, for dam breaches, the inflow decreases rapidly as the breach
58 advances and the reservoir becomes empty, whereas for the riverine levee breaches, the inflow
59 continues unless the upstream flood recedes.

60 Considering the aforementioned different characteristics of dam breach versus riverine breach, we
61 assume that the results from the dam breach experiment can be applied only to the very initial stages of
62 riverine levee breach and not to the later stages. This is because the horizontal scale versus the vertical
63 scale for riverine levee breaches may exceed 100 or more, and such scales are beyond the scope of
64 previous dam breach experiments. Therefore we realized that proper experiments were needed to
65 reproduce the riverine levee breach, which is characterized by lateral breach widening normal to river
66 flow. To obtain reliable data, we performed large-scale experiments using the Chiyoda Experimental
67 Flume (hereinafter: “the flume”).

68 The flume is in the floodway of the Tokachi River in Hokkaido, Japan, and these facilities are
69 attached to the fume, such as the inflow control gate and observation bridges. In the experiments, we
70 simulated riverine levee breaches by erecting a model levee with an overtopping notch on the right side

of the flume, and we performed four test cases with varied inflow discharges, levee materials and levee structural configurations. We studied general characteristics of the riverine breach, and also obtained hydraulic data as well as morphological data during the breach process. We also applied a two-dimensional numerical model and modified it by integrating the experimental results into the geomechanics.

Description of Experiment

Experiment facilities and test conditions

Figure 1 is an aerial photo of the flume. The flume specifications are shown in Figure 2. We constructed the flume on the floodway channel of the Tokachi River, with a separation levee on the right side and vertical steel sheet piles on the left side. The bed slope was approximately 1/500. We also created an overflow area with a width of 80 m or more on the right side using part of the floodway channel. In the breach experiment section, we replaced a portion of the separation levee with a model levee that is made of homogeneous material and with a bare surface (an embankment with no turf) and a rectangular notch, 0.5 m in depth and 3 m in width, to trigger a breach. We constructed a dam-up facility at the downstream end of the flume to maintain the proper water level. To prevent bank erosions, we placed revetment works on the upstream slope side of the levee breach experiment section.

The test cases have variations in inflow discharge, levee configuration (crest width) and levee materials, as shown in Table 1. The grain size distribution curves of the levee materials are shown in Figure 3. The bed material was roughly similar to the materials in Cases 1 and 2.

Measurement method

We placed water level sensors every 25 m in the Flume and every 40 m in the overflow area along the levee. We also placed flow meters in the channel at 50 m upstream and 120 m downstream from the overtopping notch, respectively, so that the overflow rate could be calculated from the balance of these flow rates. We applied Particle Image Velocimetry (PIV) to measure the surface flow rate distribution at the levee breach section. A unique feature of the experiments was that we placed accelerometers inside the levee body and substrata to monitor the breach process under overflowing water. The accelerometers were installed at intervals of 1.5 m in the cross-sectional and vertical directions, and 2 m in the longitudinal direction.

Test Results

Water level observation

The results of water level observations in the flume and the overflow area are shown in Figure 4 (top). Dotted lines indicate the notch height, and dashed lines indicate the time at which the gate closing began. In each case, the water level rose until it reached the target height and remained constant for a while. When the breach began to widen laterally, the water level fell and then kept constant. The tail water level in the overflow area began to rise when the head water level fell, and the difference between these water levels decreased. As indicated by the correlation between the head water level and the breach width, when the width was approximately 10 m in Cases 1 and 2 or 30 m in Cases 3 and 4, the head water began to fall and the water flowed quickly into the levee breach opening.

Flow rate observation

Figure 4 (middle) shows the flow rates in the upstream and the downstream of the levee breach section, as well as the overflow rates, which we calculated from the balance of the upstream and the downstream flow rates with consideration of increase or decrease of the water storage quantities in the breach section of the flume. The overflow rate increased a little at the initial overtopping stage in each case and began to increase significantly when breach widening was initiated. After the overflow rate peaked, it remained roughly constant until the gate was closing and the inflow began to decrease.

Levee breach observation

Figure 4 (bottom) shows the time history of the breach width along the center of the levee crest as measured by video images taken from above. The vertical axis indicates the distance from the notch, where plus means downstream direction and minus means upstream direction. The longitudinal axis indicates the time elapsed from the beginning of initial overtopping. The levee breach process was monitored by the accelerometers, and Figure 5 shows a time series of breach opening shapes for Case 1, which we estimated from the accelerometer results. The black dots indicate the position of the sensors that flowed out.

Characteristics of Breach Process

Beginning of levee breach

As shown in Figure 5, the initial breach stage began with downstream slope erosion. The erosion retrograded from the top of the downstream slope to the top of the upstream slope. After the erosion reached the top of the upstream slope, the breach opening began to widen gradually in the upstream and downstream directions. A similar process was seen in the other cases. As shown in Figure 4 (bottom), this initial stage took longer in Cases 3 and 4 than in Case 1. We assumed that the factor causing this for Case 3 was the relatively higher soil cohesion, which may have slowed the erosion processes, and that the factor causing this for Case 4 was the larger cross-sectional volume of the levee to be eroded.

Here we must mention that the notch placed on the levee top might have affected the processes in the beginning stages. So further studies are needed to clarify the experiments could reproduce the early stages correctly or not.

Lateral widening of breach opening

As shown in Figure 4 (bottom) and mentioned in the previous chapter, the breach opening began to widen gradually in the upstream and the downstream directions. Then, the opening began to widen in the downstream direction very rapidly. The rate of widening speed kept almost constant for a while. In Case 2 where the inflow was low, the rate of widening speed was lower than other cases. In Case 3 where the levee material was relatively fine, the levee collapsed in bulk repeatedly and the rate of breach widening was higher than for other cases of coarse material.

Next, we examined the process of side breaching in detail. From the observations, we noticed that the lower part of the levee, which was hit by the water first, failed and subsequently the upper part lost support and collapsed. Comparing the timing of breaching at the crest (measured by video image from above) and below the crest (measured by accelerator sensors) at the same cross-section, we realized that

the whole structure in every case breached almost simultaneously. Also, we realized that in Case 4 the slightly remained lowest structure and the substrata were degraded later than the breach.

Another characteristic we found was that the downstream slope side failed before the upstream slope side.

Levee breach and sedimentation process

Comparing Figure 4 (middle) and Figure 4 (bottom), even when the overflow rate was nearly constant in the later stage, the breach widening continued. We estimate the reasons as follows. Figure 6 shows the surface flow rate distributions for Case 3 from PIV observation. A narrow band of high-velocity flow, 4 m/s or more, appeared and struck the side of the breached levee. When the breach width reached approximately 30 m, the band became nearly half the entire breach width. Even when the breach width reached approximately 50 m, the width of the band remained roughly the same as before, and a dead-water area appeared near the upstream end of the breach opening where deposition may have occurred. We summarize this process as follows. The high-velocity band erodes the levee side and moves in the downstream direction, then, sedimentation occurs in the upstream area. This repeated process makes the breach widen in the downstream direction as the band moves downstream, keeping almost constant width.

Summary of breach process stage

In consideration of the breach processes observed in the tests, we categorized the levee breach process into the four stages shown in Figure 7.

186

187 ## Quantitative Evaluation of Breach Process

188

189 ### *Formula for breach morphology*

190

191 As mentioned in Chapter 1, the main purpose of this study is the evaluation of the breach lateral
192 widening process toward developing a numerical riverine breach model. Therefore we focused on the
193 3rd and 4th breach stages for analyzing the breach widening process. Although we mentioned in
194 Chapter 4.2 that the breach process of the upper part of the levee differs from that of the lower part, as
195 shown in Figure 8, we assumed that both parts would be subject to the same mechanism, because the
196 upper part collapses onto the foot of the lower part and then washes out by the flow, which is the same
197 mechanism as for the lower part. Therefore we also assumed that the total volume of breached levee
198 transported per unit time and width (hereinafter: "breached load transport") could be expressed by a
199 kind of the sediment load transport formula, and we proposed eq. (1) with reference to the Meyer-Peter
200 and Müller equation

201 $$q_B = \alpha(\tau_* - \tau_{*_c})^{\beta}\sqrt{sgd^3} \quad (1)$$

202 where q_B= breached load transport; α and β are coefficients; τ_*= Shields number; τ_{*c}= critical Shields
203 number; s= submerged specific sediment density; g= gravitational acceleration; and d= mean diameter
204 of the levee material. Then q_B can be calculated from the experimental results as

205 $$q_B = (1-\lambda)\frac{dV}{dt}\frac{1}{L} \quad (2)$$

206 $$\frac{dV}{dt} = \frac{dV_1}{dt} + \frac{dV_2}{dt} \quad (3)$$

207 where V= breached volume; V_1= breached volume for the lower part; V_2= breached volume for the

208 upper part; t= time; λ= porosity of the levee material; and L= characteristic length.

209 Then we obtained α and β through the comparison of eq. (1) and (2).

210

211 *Analysis of test results*

212 We applied the experimental results to eq. (1) and (2), to obtain α and β as follows. We assumed λ

213 should be 0.4, d should be d_{50}, and s should be 1.65. Then we calculated dV/dt ($=dV_1/dt+dV_2/dt$) every 5

214 minutes from the acceleration sensor data. The results are shown in Figure 9. Shields number τ_* is

215 calculated as

216 $$\tau_* = \frac{N_m{}^2 u_m^2}{sdh^{\frac{1}{3}}} \quad (4)$$

217 where N_m= manning's roughness coefficient (=0.023); u_m= depth-averaged overflow velocity; and h=

218 water depth. We set a value for the flow velocity u_m as the surface flow rate measured by PIV near the

219 downstream slope of the breach opening end where the flow struck and eroded the levee. We also set a

220 value for the water depth h calculating the balance of the water surface elevations measured by 3D

221 analysis and the initial bed elevations. (Bed level change should be considered but we did not have such

222 data near the downstream slope.) We set a value for the critical Shields number τ_{*c} as 0.05 by applying

223 the method of Iwagaki (1956). Lastly we applied the levee bottom width as the characteristic length.

224 We plotted the test results as shown in Figure 10. We observed different breach characteristics for

225 each test case; however, the plotted results showed a correlation expressed by the following equation

226 $$(1-\lambda)\frac{dV}{dt}\frac{1}{L}\frac{1}{\sqrt{sgd^3}} = 18(\tau_* - \tau_{*_c})^{1.5} \quad (5)$$

227 We found that the coefficient β in eq. (1) had the value of 1.5, which was similar to the value

228 appearing in sediment load transport formulas such as those of Meyer-Peter and Müller. This finding is

229 expected to be useful in the development of a levee breach model based on such a simple equation for

230 simulating the lateral widening breach process.

231

232 ## Numerical Simulation

233

234 ### *Conventional numerical model*

235

236 Faeh (2007) developed a numerical model based on shallow-water equations considering both bed
237 load and suspended load. The model also has the ability to incorporate slope stability. He evaluated the
238 ability of the model to simulate levee breaches on the Elbe River. The model was able to simulate the
239 main characteristic of the flow field, but it was found to be still limited. He also pointed out that the
240 most sensitive parameters were critical angles describing the bank failure mechanism and, thus,
241 implicitly the ratio between vertical and horizontal erosion. For the simulation of the experimental
242 result (Case 4), we assumed that suspended load could be neglected because the main levee materials
243 were sand and gravel. Therefore we employed the two-dimensional model "Nays" (Shimizu 1996, Jang
244 and Shimizu 2005, iRIC 2013), which is based on shallow-water flow and bed load transport. The
245 model also has the ability to incorporate slope stability (repose angle) for bank erosion. The governing
246 equations for the model in the orthogonal coordinate system are given as follows,

247 [Continuity equation for flow]

248 $$\frac{\partial h}{\partial t}+\frac{\partial (hu)}{\partial x}+\frac{\partial (hv)}{\partial y}=0 \quad (6)$$

249 [Momentum equation for flow]

250 $$\frac{\partial u}{\partial t}+u\frac{\partial u}{\partial x}+v\frac{\partial u}{\partial y}=-g\frac{\partial H}{\partial x}-\frac{C_f u}{h}\sqrt{u^2+v^2}+\nu_t\left(\frac{\partial^2 u}{\partial x^2}+\frac{\partial^2 u}{\partial y^2}\right) \quad (7)$$

$$\frac{\partial v}{\partial t}+u\frac{\partial v}{\partial x}+v\frac{\partial v}{\partial y}=-g\frac{\partial H}{\partial y}-\frac{C_f v}{h}\sqrt{u^2+v^2}+\nu_t\left(\frac{\partial^2 v}{\partial x^2}+\frac{\partial^2 v}{\partial y^2}\right) \quad (8)$$

[Sediment transport equation]

$$q_b=8\left(\tau_*-\tau_{*_c}\right)^{1.5} \quad (9)$$

$$q_b^x=\frac{u}{\sqrt{u^2+v^2}}q_b\,,\ q_b^y=\frac{v}{\sqrt{u^2+v^2}}q_b \quad (10)$$

[Continuity equation for sediment]

$$\frac{\partial Z_b}{\partial t}+\frac{1}{1-\lambda}\left(\frac{\partial q_b^x}{\partial x}+\frac{\partial q_b^y}{\partial y}\right)=0 \quad (11)$$

where x, y are orthogonal coordinates; h=water depth; t=time; u, v are velocity in the x and y directions, respectively; H=water level elevation; C_f=riverbed shear coefficient; ν_t=eddy viscosity coefficient; q_b=total bed load transport per unit width; q_b^x, q_b^y are bed load transport per unit width in the x and y directions, respectively; Z_b=riverbed elevation; λ=porosity of the levee material.

It is useful to write the sediment transport equation in the general coordinate system because we modify the equation in the general coordinate system later in this paper.

$$\frac{\partial}{\partial t}\left(\frac{Z_b}{J}\right)+\frac{1}{1-\lambda}\left\{\frac{\partial}{\partial \xi}\left(\frac{q_b^\xi}{J}\right)+\frac{\partial}{\partial \eta}\left(\frac{q_b^\eta}{J}\right)\right\}=0 \quad (12)$$

where ξ, η are general coordinates; q_b^ξ, q_b^η are bed loads transport in the ξ and η directions, respectively; J= jacobian of the coordinate transformation.

Figure 11 shows the calculation area and the boundary conditions. In the simulations, we made a set of elevation data of the flume, the notched levee, and the overflow area for geographical input data to reproduce Case 4. We also simulated inflow as the experimental result of Case 4. Then we made the calculation settings shown in Table 2. We set the grid size as 1 m by 1 m for Run 1, 2, and 3.

Figure 12 shows the time history of the breached volume for each calculation run and the experimental result. The experiment took longer time in the early stage which could not be reproduced by calculation, so we shift the experimental result so that the data starts from the beginning of breach widening. Focusing on the breach widening speed, Run 1 (repose angle of 30 degrees) reproduced better results but was still slower than the experimental result. Numerical models using critical failure angles are known to depend strongly on a fine grid size, therefore we calculated Run 4, in which the grid size was 0.5 m by 0.5 m. Run 4 showed almost the same result as Run 1, so we recognized that the grid size of 1 m by 1 m was reasonable.

Next, we analyzed the simulation results and observed breach mechanisms. As observed in the experiment, the lower part of the levee hit by the water was eroded laterally and the levee side surface of the collapsed part is very steep (almost 90 degrees). However, the numerical model neither includes a lateral erosion mechanism nor does the repose angle reflect the observation results. In the breach widening stage, the lateral erosion process becomes the primary mechanism of breach. Therefore we suppose that improved lateral erosion formulas need to be developed.

Proposed model

We modified only formulas relating morphodynamics in the aforementioned model. Instead of using the sediment transport formula and the slope stability model, we brought an empirical formula delivered from the experimental results. First, we separate the calculation cells of the levee (except near the notch) from other cells. We call the former “levee cells” and the latter “normal cells”. For the levee cells, we propose a breach rate formula which is different from the sediment transport formula for the normal cells. Referring to the eq. (5), we assume the breached loads to be collapsed in the orthogonal

direction of the streamline as eq. (13) and (14). The breached loads are to be placed on adjacent normal cells and to be transported using the original transport formulas from the next time step. Figure 13 shows the streamline and coordinate systems.

$$q_v^n = \frac{1-\lambda}{L}\frac{dV}{dt} = 18\sqrt{sgd^3}\left(\tau_* - \tau_{*_c}\right)^{1.5} \quad (13)$$

$$q_v^s = 0 \quad (14)$$

where q_v^n = breached loads orthogonal to the streamline; and q_v^s = breached loads along the streamline. As for the characteristic length L, it can be represented by the calculation cell width.

Here we describe the detailed calculation processes for breached loads. Referring to the governing equations developed by Jang and Shimizu (2005), we transform q_v^s and q_v^n into the general coordinate system as

$$q_v^\xi = \left(\frac{\partial x}{\partial s}\frac{\partial \xi}{\partial x} + \frac{\partial y}{\partial s}\frac{\partial \xi}{\partial y}\right)q_v^s + \left(\frac{\partial x}{\partial n}\frac{\partial \xi}{\partial x} + \frac{\partial y}{\partial n}\frac{\partial \xi}{\partial y}\right)q_v^n = \left(\cos\theta_s\xi_x + \sin\theta_s\xi_y\right)q_v^s + \left(-\sin\theta_s\xi_x + \cos\theta_s\xi_y\right)q_v^n \quad (15)$$

$$q_v^\eta = \left(\frac{\partial x}{\partial s}\frac{\partial \eta}{\partial x} + \frac{\partial y}{\partial s}\frac{\partial \eta}{\partial y}\right)q_v^s + \left(\frac{\partial x}{\partial n}\frac{\partial \eta}{\partial x} + \frac{\partial y}{\partial n}\frac{\partial \eta}{\partial y}\right)q_v^n = \left(\cos\theta_s\eta_x + \sin\theta_s\eta_y\right)q_v^s + \left(-\sin\theta_s\eta_x + \cos\theta_s\eta_y\right)q_v^n \quad (16)$$

where q_v^ξ = breached loads in the ξ direction; and q_v^η = breached loads in the η direction; θ_s = angle of the streamline to the *x*-axis as given by eq. (17) and (18); and $\xi_x = \partial\xi/\partial x$, $\xi_y = \partial\xi/\partial y$, $\eta_x = \partial\eta/\partial x$,and $\eta_y = \partial\eta/\partial y$.

$$\sin\theta_s = -\frac{\partial x}{\partial n} = \frac{\partial y}{\partial s} = \frac{v}{U}, \cos\theta_s = \frac{\partial y}{\partial n} = \frac{\partial x}{\partial s} = \frac{u}{U} \quad (17)$$

$$U = \sqrt{u^2 + v^2} \quad (18)$$

where *U*= composite velocity. From eq. (13), (14), (15), and (16), we obtain the breached loads of the general coordinates as

312 $$q_v^{\xi} = \left(-\sin\theta_s\xi_x + \cos\theta_s\xi_y\right)q_v^n = \left(-\sin\theta_s\xi_x + \cos\theta_s\xi_y\right)\left\{18\sqrt{sgd^3}\left(\tau_* - \tau_{*_c}\right)^{1.5}\right\} \quad (19)$$

313 $$q_v^{\eta} = \left(-\sin\theta_s\eta_x + \cos\theta_s\eta_y\right)q_v^n = \left(-\sin\theta_s\eta_x + \cos\theta_s\eta_y\right)\left\{18\sqrt{sgd^3}\left(\tau_* - \tau_{*_c}\right)^{1.5}\right\} \quad (20)$$

314 The breach rate formula is given as

315 $$\frac{\partial}{\partial t}\left(\frac{Z_L}{J}\right) + \frac{1}{1-\lambda}\left\{\frac{\partial}{\partial\xi}\left(\frac{q_v^{\xi}}{J}\right) + \frac{\partial}{\partial\eta}\left(\frac{q_v^{\eta}}{J}\right)\right\} = 0 \quad (21)$$

316 where Z_L= levee cell elevation; J= jacobian of the coordinate transformation. When applying this
317 formula, Shields numbers are set as the largest value within 4 m from the levee cell in the same way of
318 the experiment analysis. When the elevation of a levee cell comes below the riverbed, the cell becomes
319 a normal cell.

320 Table3 shows the calculation conditions. Figure 14 shows the calculation results of time-series
321 breached volume by the proposed model (Run 5). The model could not reproduce the early stage, but
322 when comparing the widening stage, the proposed model is found to be improved in terms of breach
323 widening speed and total volume. Next, we conducted some other comparisons of the test result and the
324 calculation result. Figure 15 shows comparisons of levee breach shapes and the flow distributions at the
325 same stage, and they are found to be well reproduced. Figure 16 shows comparisons of overflow
326 discharges and stage hydrographs at the channel center near the notch, and they are reasonably
327 reproduced except discharge in the early timing.

328 Lastly, we checked the sensitivity by the constant values. Figure 14 also shows the calculation results
329 using various values of α and β. We found that the value of β affect greater than the value of α, which
330 can be supposed from the eq. (13).

331

332 *Limitations and future improvement of modeling*

333 The scope of our study is to reproduce the breach widening stage, so the poor performance by the

model in the early stage is not focused on. However, we recognize the importance to simulate the early stage of the breach. In the early stage, the flow and sediment interaction is significant like dam breaks, so the dam break models can be appropriate to use for the initial stage. Xia et al. (2010) used a coupled approach to solve simultaneously the flow and sediment transport processes induced by dam breaks. To applying coupled approach for the initial stage may be a future challenge. Furthermore we need investigations to find parameters for various levee materials or levee shapes other than the experiment conditions we performed in order to apply the model to real rivers.

Conclusions

1. We performed large-scale levee breach experiments and identified several characteristics of the breach process using sensors placed in the levee structure.
2. We categorized the breach processes into four stages. The breach began with downstream slope erosion (1st stage). After the erosion reached the top of the upstream slope, the breach opening began to widen gradually (2nd stage). The breach widened in the downstream direction rapidly and the overflow rate became maximum (3rd stage). The overflow rate kept constant and the breach rate decreased (4th stage).
3. We identified the breach widening mechanism, focusing on sedimentation and overflow distribution. The narrow and strong overflow produced by combination of breach and deposition eroded the levee side and moved in the downstream direction.
4. We identified a correlation equation to estimate the volume of breached levee.
5. We understand the importance of spiral flow effect, which could be crucial to determine the lateral breaching process. However, we proposed modifying two-dimensional numerical model which

cannot replicate such effect physically, and thus it has to be parameterized in some way, therefore we integrated the empirical correlation equation delivered from the experimental result. The modified model could not reproduce the early stage but well reproduced the breach widening stage.

Notation

The following symbols are used in this paper:

q_B = breached load transport

α, β = coefficients of breached load transport formula

τ_* = Shields number

τ_{*c} = critical Shields number

s = submerged specific sediment density

g = gravitational acceleration

d = mean diameter of the levee material

V = breached volume

V_1 = breached volume for the lower part of the levee

V_2 = breached volume for the upper part of the levee

t = time

λ = porosity of the levee material

L = characteristic length.

N_m = manning's roughness coefficient

u_m = depth-averaged overflow velocity

h= water depth

380 q_v^n = breached loads orthogonal to the streamline

381 q_v^s = breached loads along the streamline

382 q_v^ξ = breached loads in the ξ direction

383 q_v^η = breached loads in the η direction

384 ξ, η = general coordinates

385 x, y = orthogonal coordinates

386 θ_s = angle of the streamline to the x-axis

387 u = velocity in the x direction

388 v = velocity in the y direction

389 U = composite velocity

390 Z_L = levee cell elevation

391 J = jacobian of the coordinate transformation

392

393 ## References

394

395 ASCE/EWRI Task Committee on Dam/Levee Breaching. (2011). "Earthen Embankment Breaching." *J.*

396 *Hydraul Eng.,* 137(12), 1549-1564.

397 Faeh, R. (2007). "Numerical modeling of breach erosion of river embankments." *J. Hydraul. Eng.*,

398 133(9), 1000–1009.

399 Hanson, G. J., Cook, K. R., and Hunt, S. L. (2005). "Physical modeling of overtopping erosion and

400 breach formation of cohesive embankments." *Trans. ASABE*, 48(5), 1783–1794.

401 Hunt, S. L., Hanson, G. J., Cook, K. R., and Kadavy, K. C. (2005). "Breach widening observations from

402 earthen embankment tests." *Trans. ASAE*, 48(3), 1115–1120.
403 iRIC (2013). "Nays." ⟨http://i-ric.org/en/introduction⟩.
404 Iwagaki, Y. (1956). "Fundamental study on critical tractive force." *Trans. JSCE*, 41, 1-21 (in Japanese).
405 Jang, C. L. and Shimizu, Y. (2005). "Numerical simulation of relatively wide, shallow channels with
406 erodible banks." *J. Hydraul. Eng.*, 131(7), 565-575.
407 Morris, M. W. and Hassan, M. A. A. M. (2005). "IMPACT: Breach formation technical report (WP2)."
408 *IMPACT*, ⟨http://www.impact-project.net⟩.
409 Sattar, A.M.A., Kassem, A.A., and Chaudhry, M.H. (2008). "Case study: 17th street canal breach,
410 closure procedures" *J. Hydraul. Eng*, 134(11).
411 Shimizu, Y., Hirano, N., and Watanabe, Y. (1996). "Numerical calculation of bank erosion and free
412 meandering." *Annu. J. Hydr. Engrg., JSCE*, 40, 921–926 (in Japanese).
413 Wahl, T. L. (2007). "Laboratory investigations of embankment dam erosion and breach processes." *Rep.*
414 *T032700-0207A, EA Technologies, Inc. (CEATI)*, Montréal.
415 Xia, J., Lin, B., Falconer, R. A., and Wang, G. (2010). "Modelling dam-break flows over mobile beds
416 using a 2D coupled approach." *Advances in Water Resources*, Vol.33, 2, 171-183.

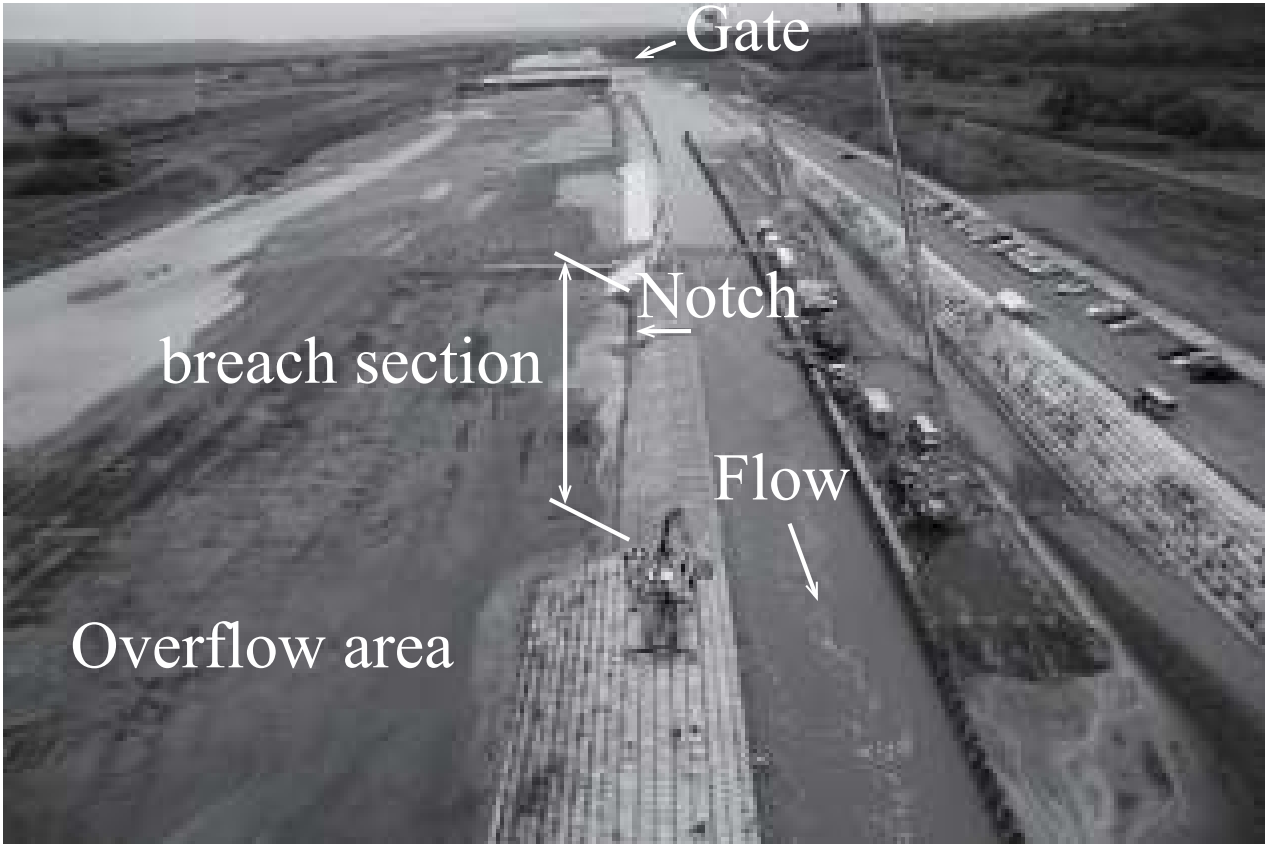
Gate
Notch
breach section
Flow
Overflow area

Case1, 2, 3(Case4)

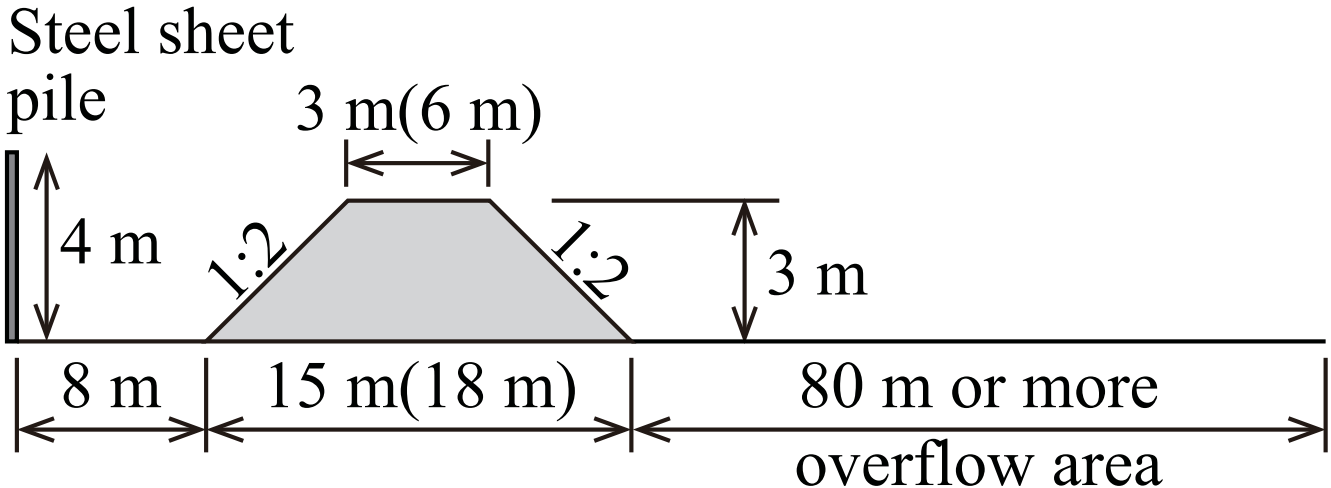

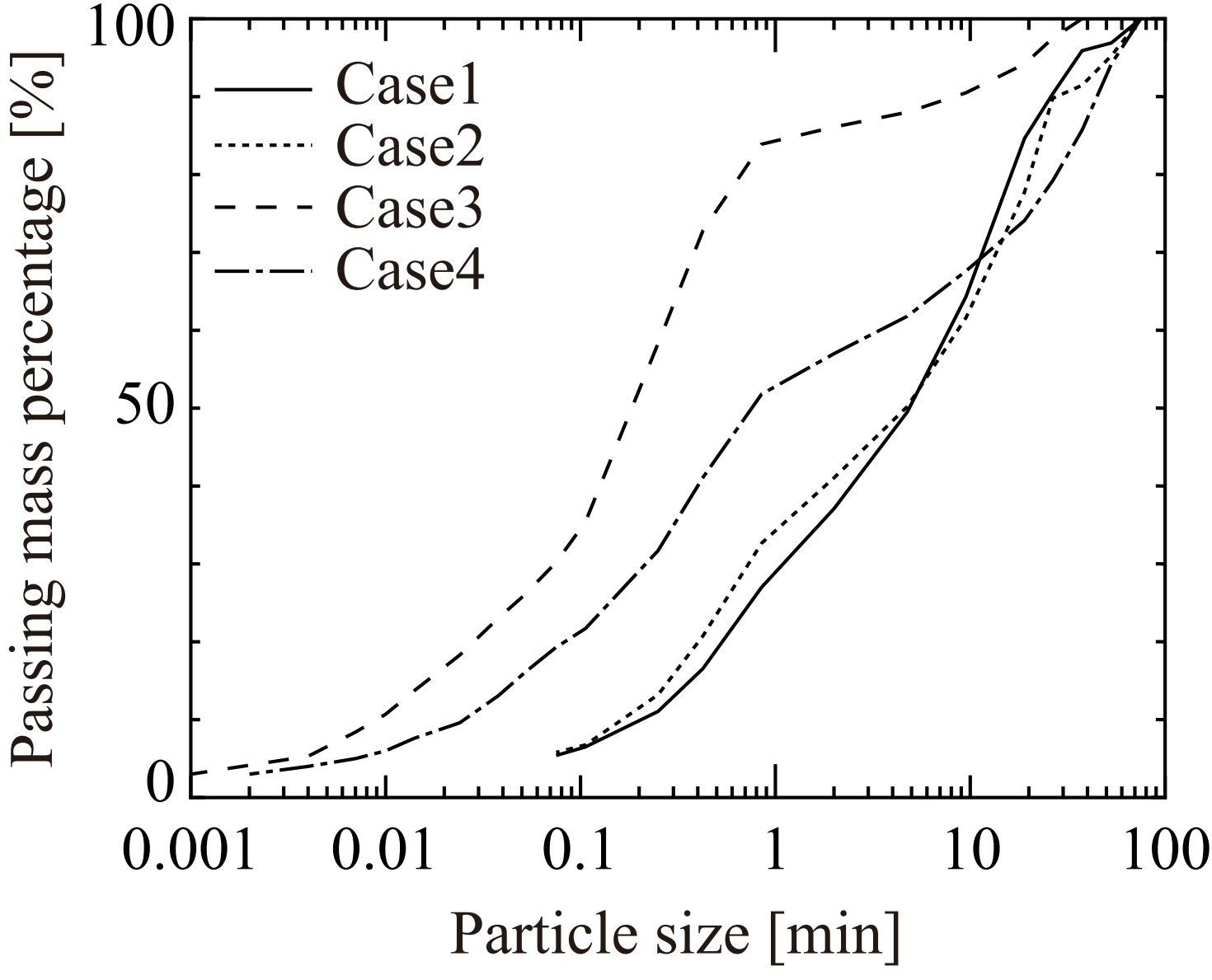
100
50
0
Passing mass percentage [%]
Case1
Case2
Case3
Case4
0.001
0.01
0.1
1
10
100
Particle size [min]

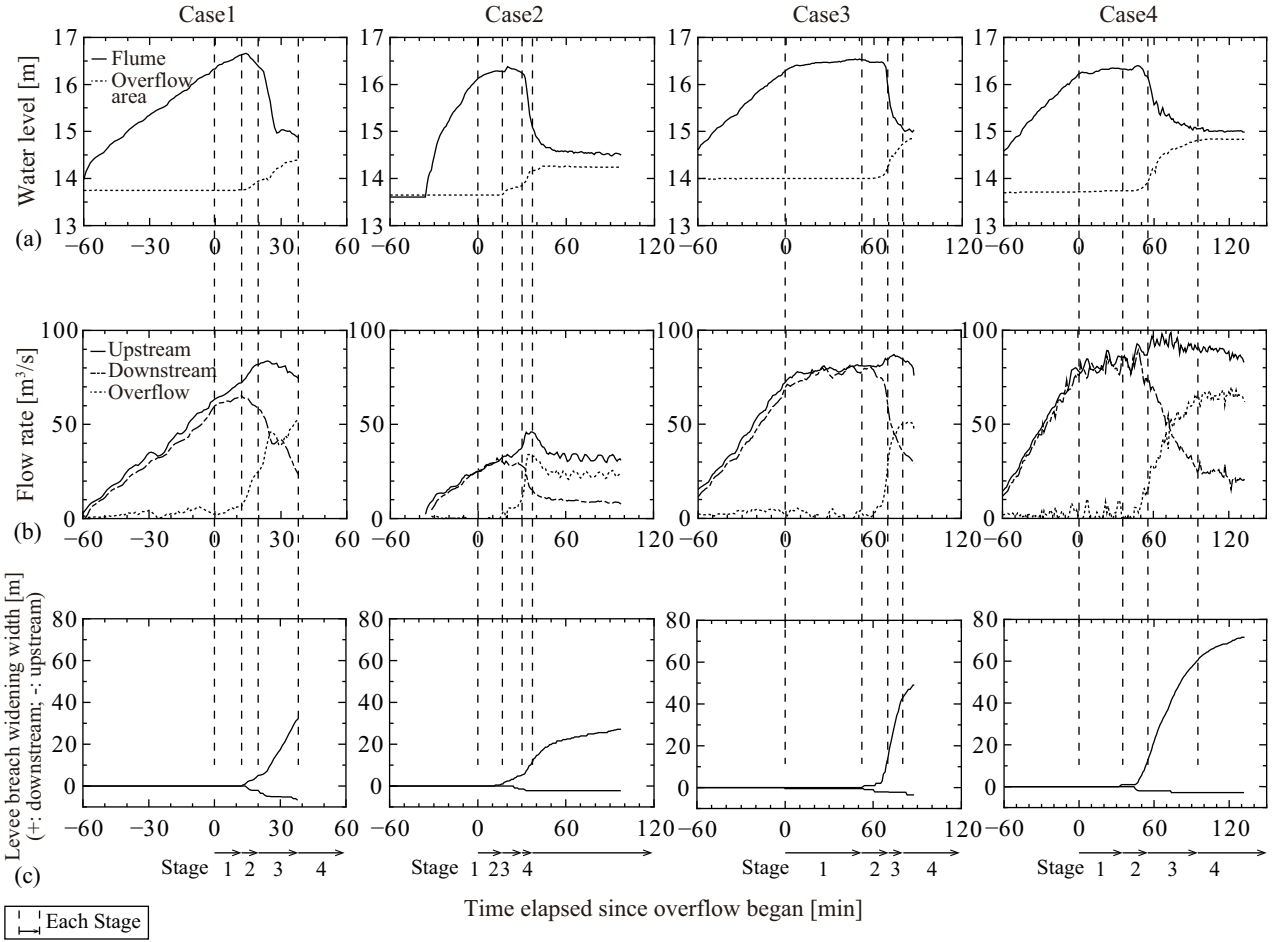
Case1
Case2
Case3
Case4
Water level [m]
Flume
Overflow area
(a)
Flow rate [m³/s]
Upstream
Downstream
Overflow
(b)
Levee breach widening width [m]
(+: downstream; -: upstream)
(c)
Stage 1 2 3 4
Stage 1 23 4
Stage 1 2 3 4
Stage 1 2 3 4
Each Stage
Time elapsed since overflow began [min]

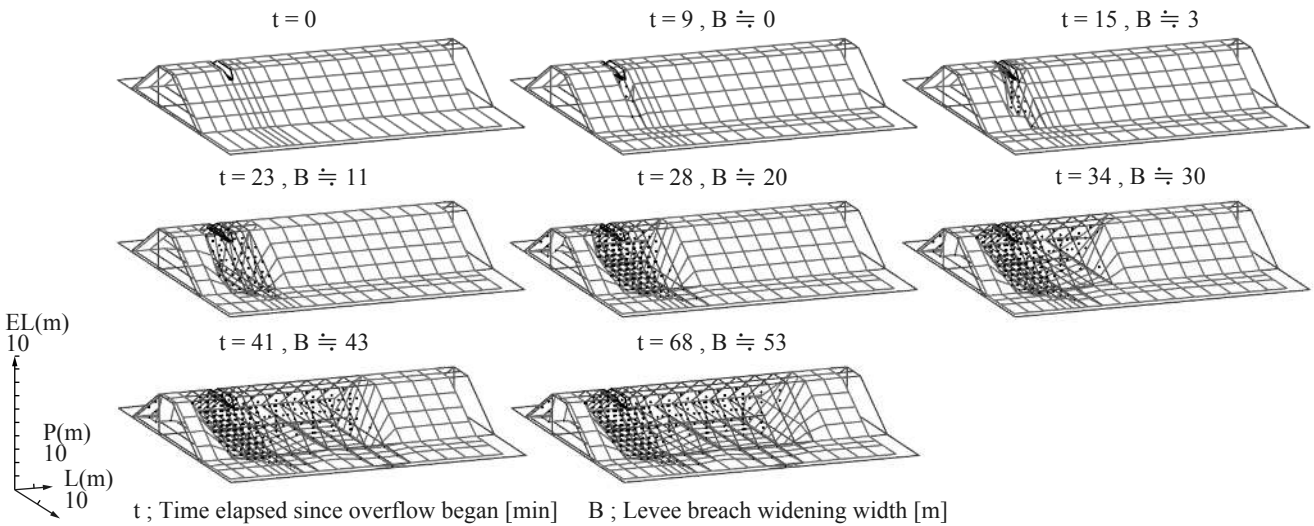
t = 0
t = 9 , B ≒ 0
t = 15 , B ≒ 3
t = 23 , B ≒ 11
t = 28 , B ≒ 20
t = 34 , B ≒ 30
t = 41 , B ≒ 43
t = 68 , B ≒ 53
EL(m)
10
P(m)
10
L(m)
10
t ; Time elapsed since overflow began [min]
B ; Levee breach widening width [m]

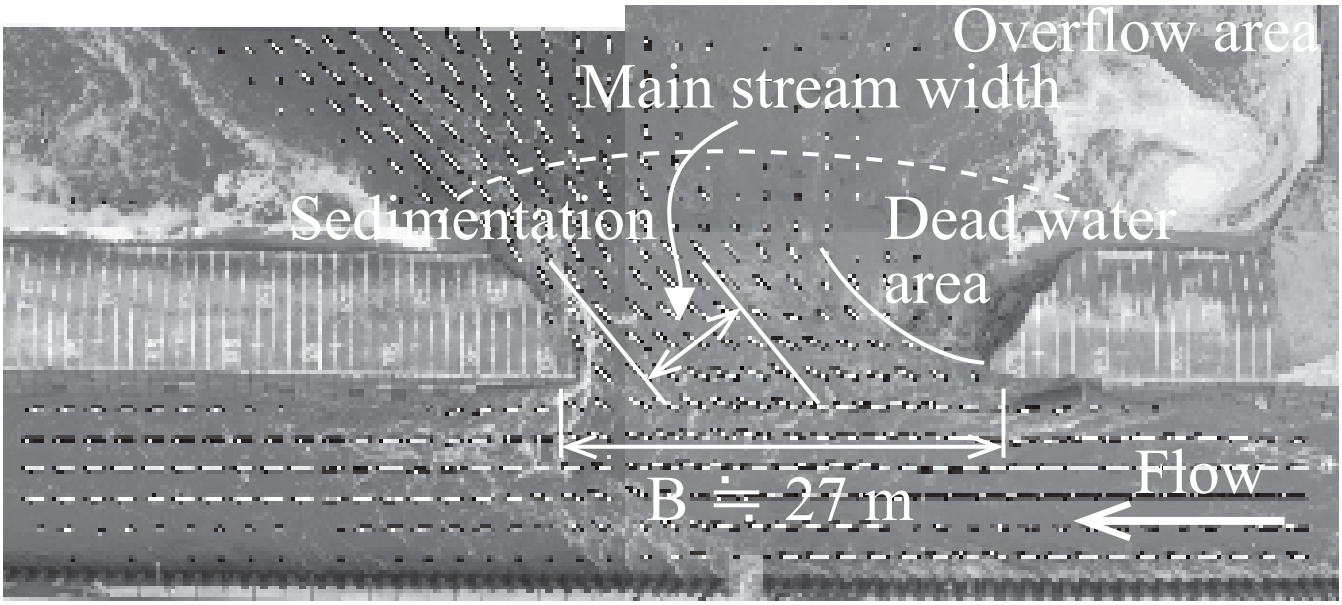

Levee breach widening width B ≒ 27 m

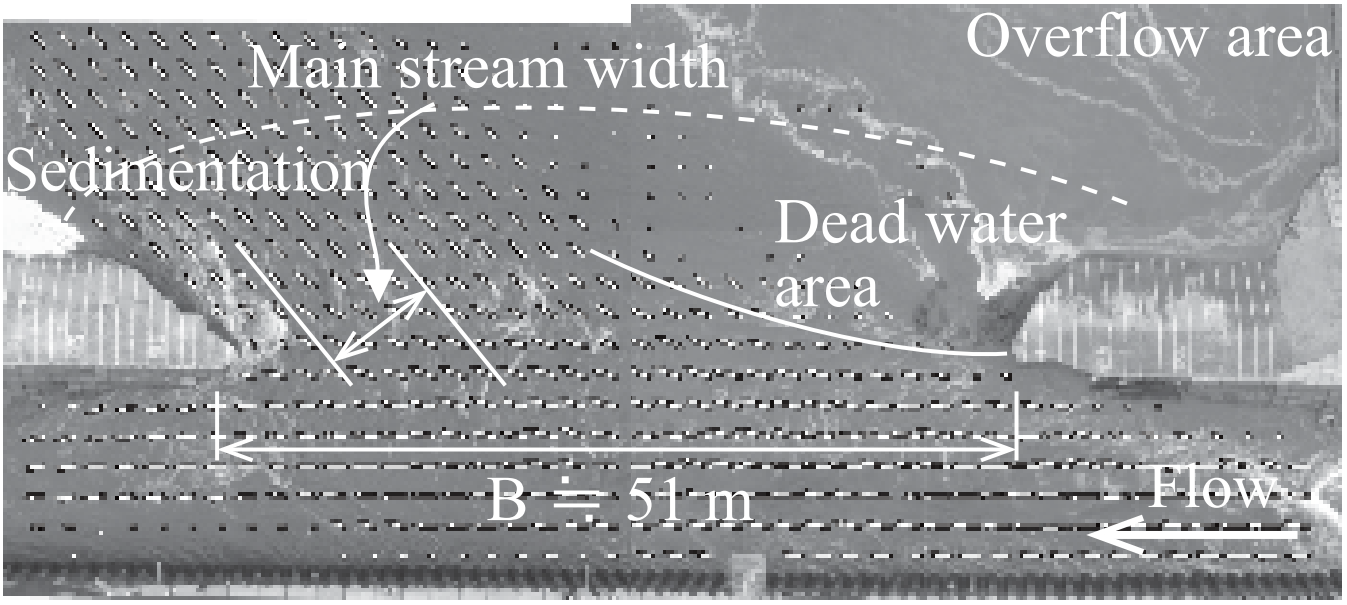

Levee breach widening width B ≒ 51 m

Legend for PIV flow rates 0 10m/s

Stage 1 (Initial levee breach)

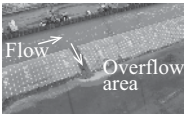

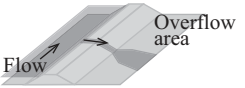

- The back slope and the top of the back slope of the levee were eroded after overflow began.
- The crown was eroded from the top of the back slope to the top of the front slope.
- The breach widening did not proceed and the overflow rate did not increase.

Stage 2 (Onset of widening)

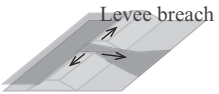

- When the top of the front slope was eroded, the erosion proceeded rapidly downward to the bottom of the levee. Then breach progressed in the upstream and downstream directions.
- The overflow rate began to increase.

Stage 3 (Acceleration of widening)

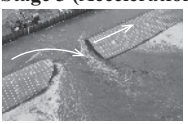

- Once most of the cross-section of levee where the notch located was eroded, the levee breach mainly progressed rapidly in the downstream direction.
- The flow from the flume to the breach opening became stronger and the flow rate increased, then the overflow rate increased and peaked.
- The overflow velocity from the breached part of the levee increased,and this flow hit and breached the levee in the downstream direction.

Stage 4 (Deceleration of widening)

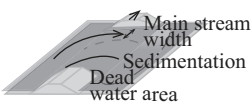

- The levee breach continued and sediment accumulated in the overflow area repeatedly, and the mainstream of the overflow shifted downstream keeping almost the same width
- The overflow rate was almost constant and the rate of breach widening decreased.
- The downstream end of the breached part of the levee slanted significantly to the overflow area and levee breach progressed.

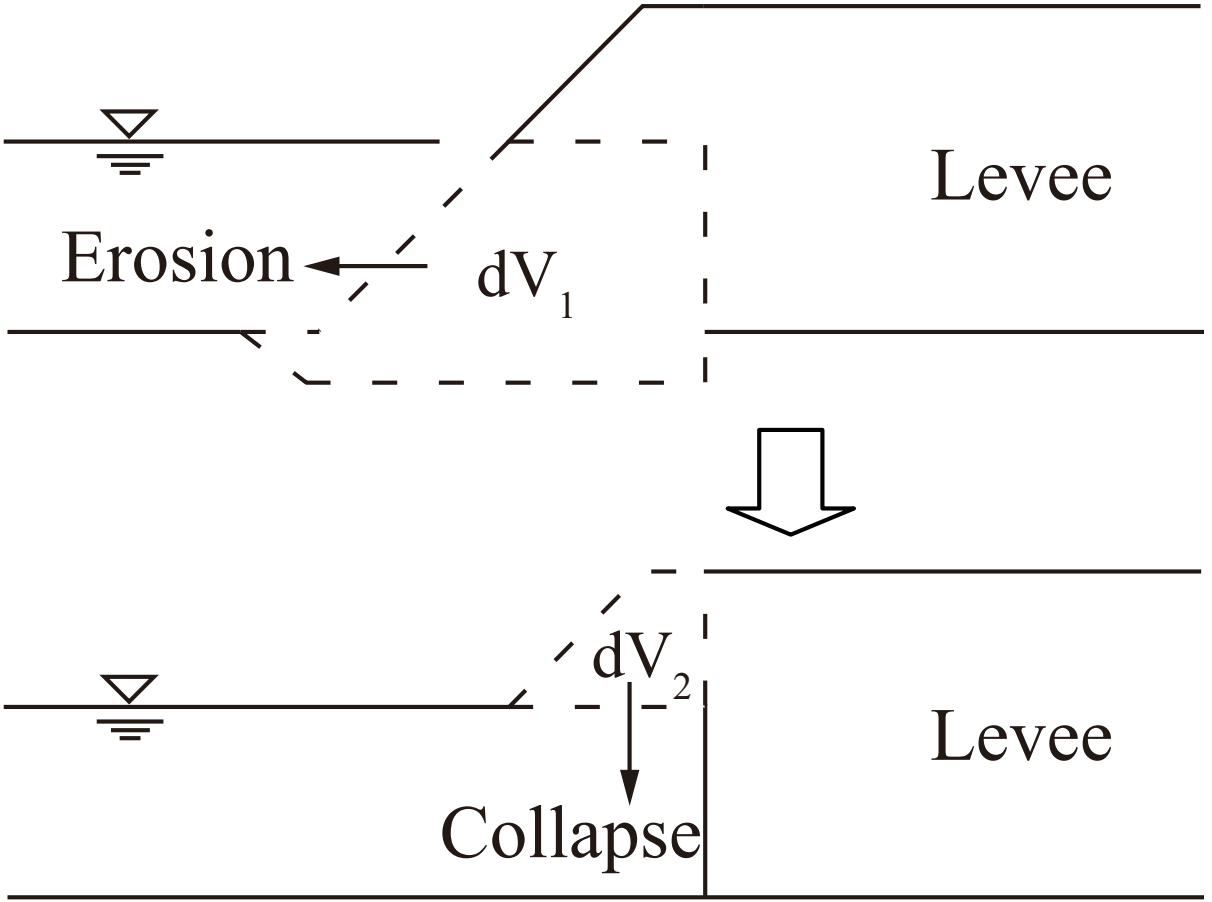
Levee
Erosion
dV1
dV2
Levee
Collapse

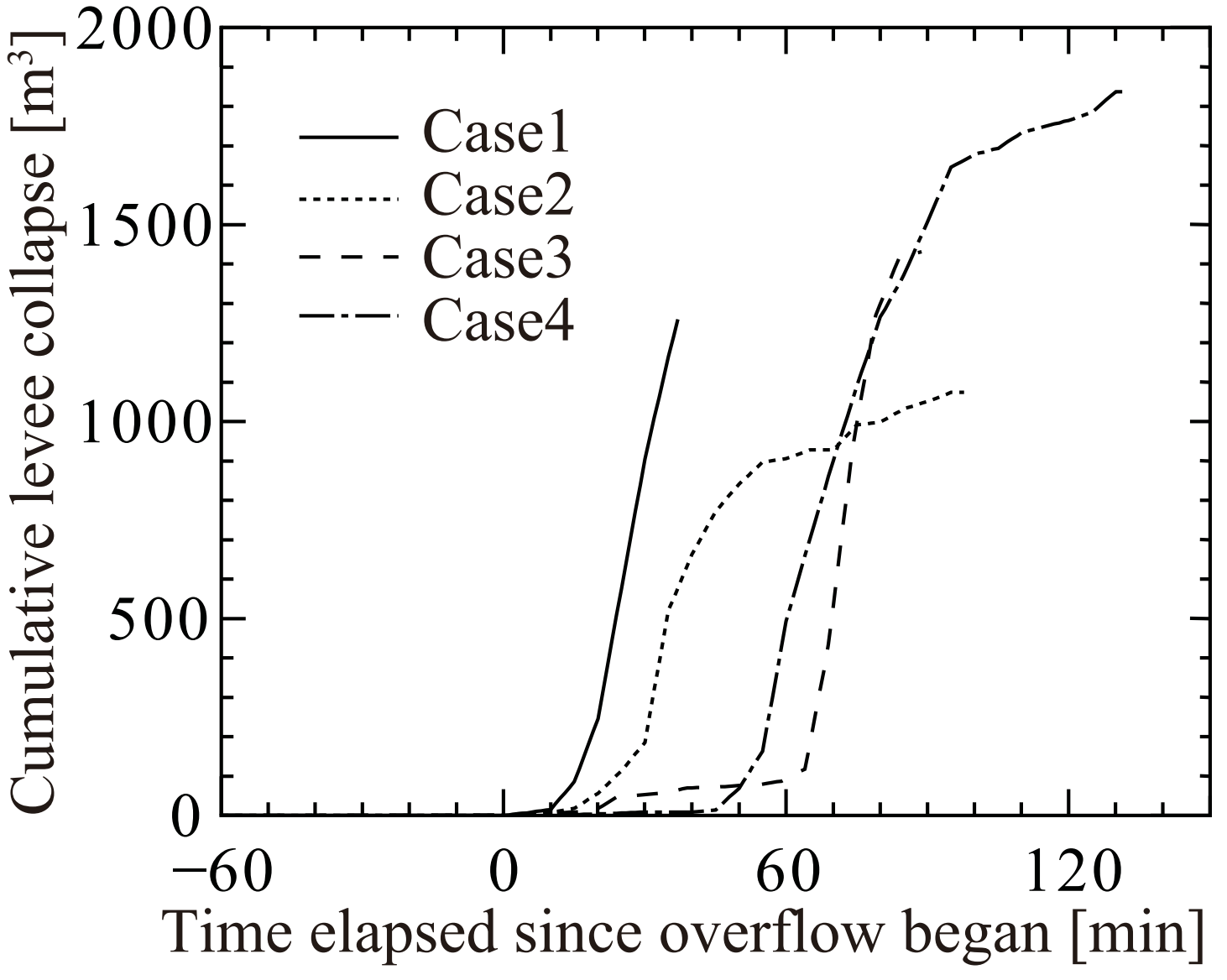
Cumulative levee collapse [m3]
2000
1500
1000
500
0
Case1
Case2
Case3
Case4
−60
0
60
120
Time elapsed since overflow began [min]

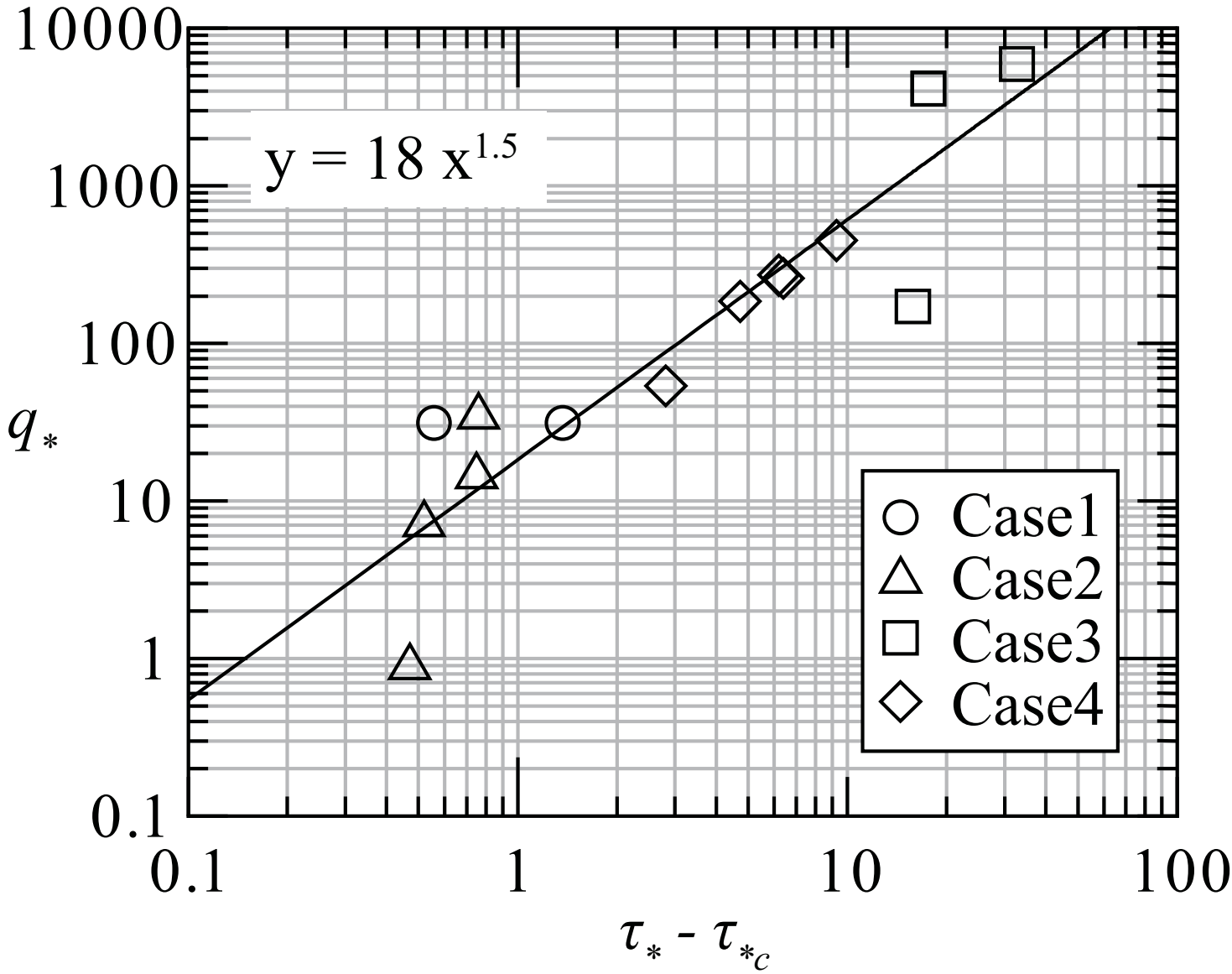
10000
1000
100
10
1
0.1
0.1
1
10
100
q_*
$\tau_* - \tau_{*_c}$
y = 18 x^1.5
Case1
Case2
Case3
Case4

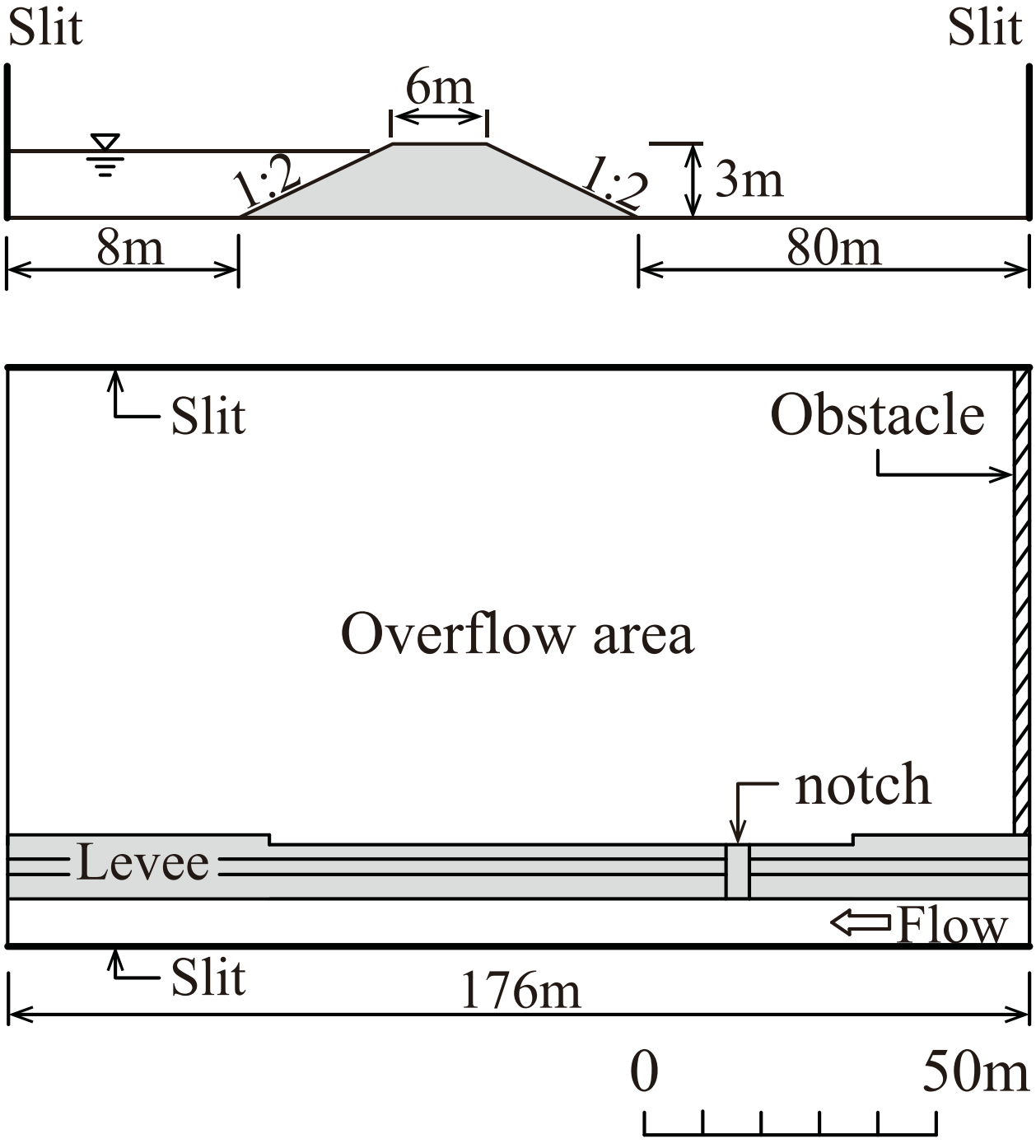
Slit
Slit
6m
1:2
1:2
3m
8m
80m
Slit
Obstacle
Overflow area
notch
Levee
Flow
Slit
176m
0
50m

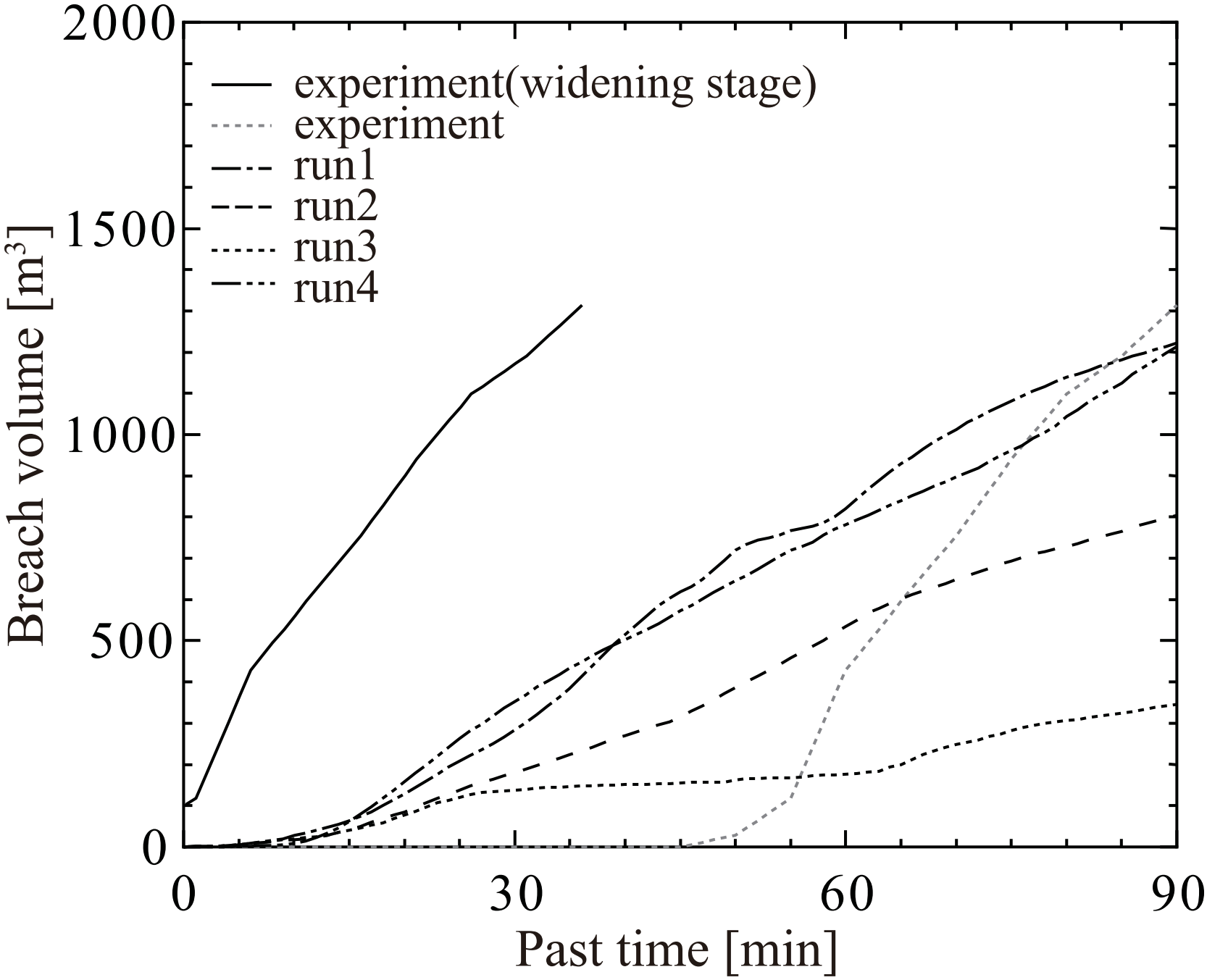
2000
1500
1000
500
0
Breach volume [m3]
0
30
60
90
Past time [min]
experiment(widening stage)
experiment
run1
run2
run3
run4

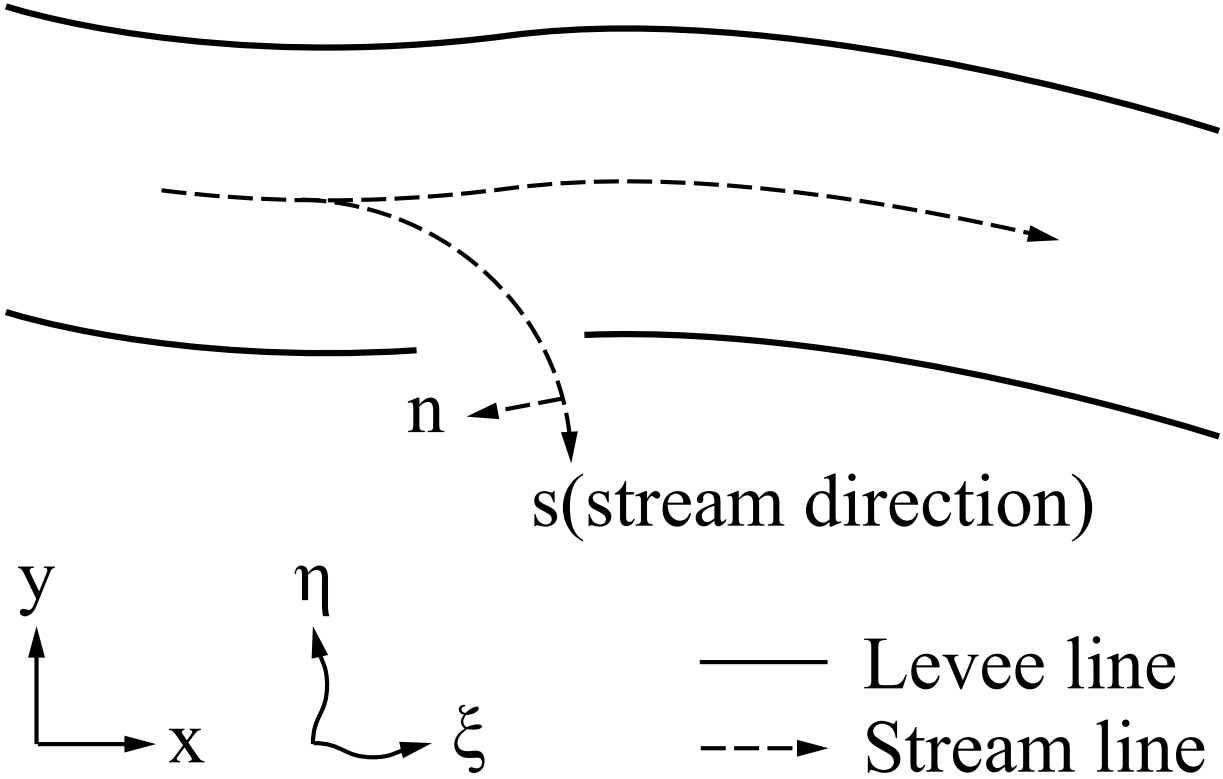
n
s(stream direction)
y
x
η
ξ
Levee line
Stream line

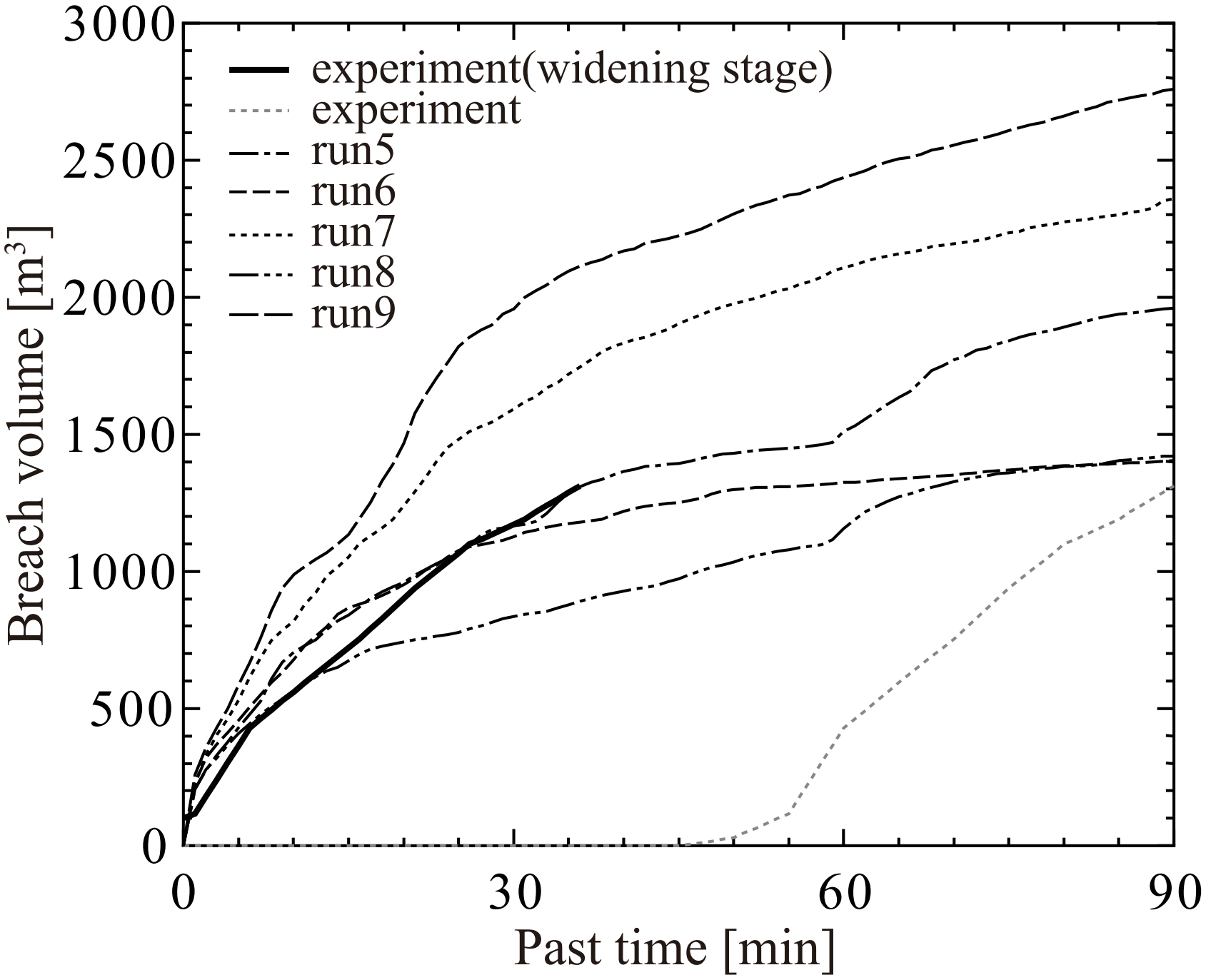
experiment(widening stage)
experiment
run5
run6
run7
run8
run9
Breach volume [m3]
Past time [min]
0
500
1000
1500
2000
2500
3000
0
30
60
90

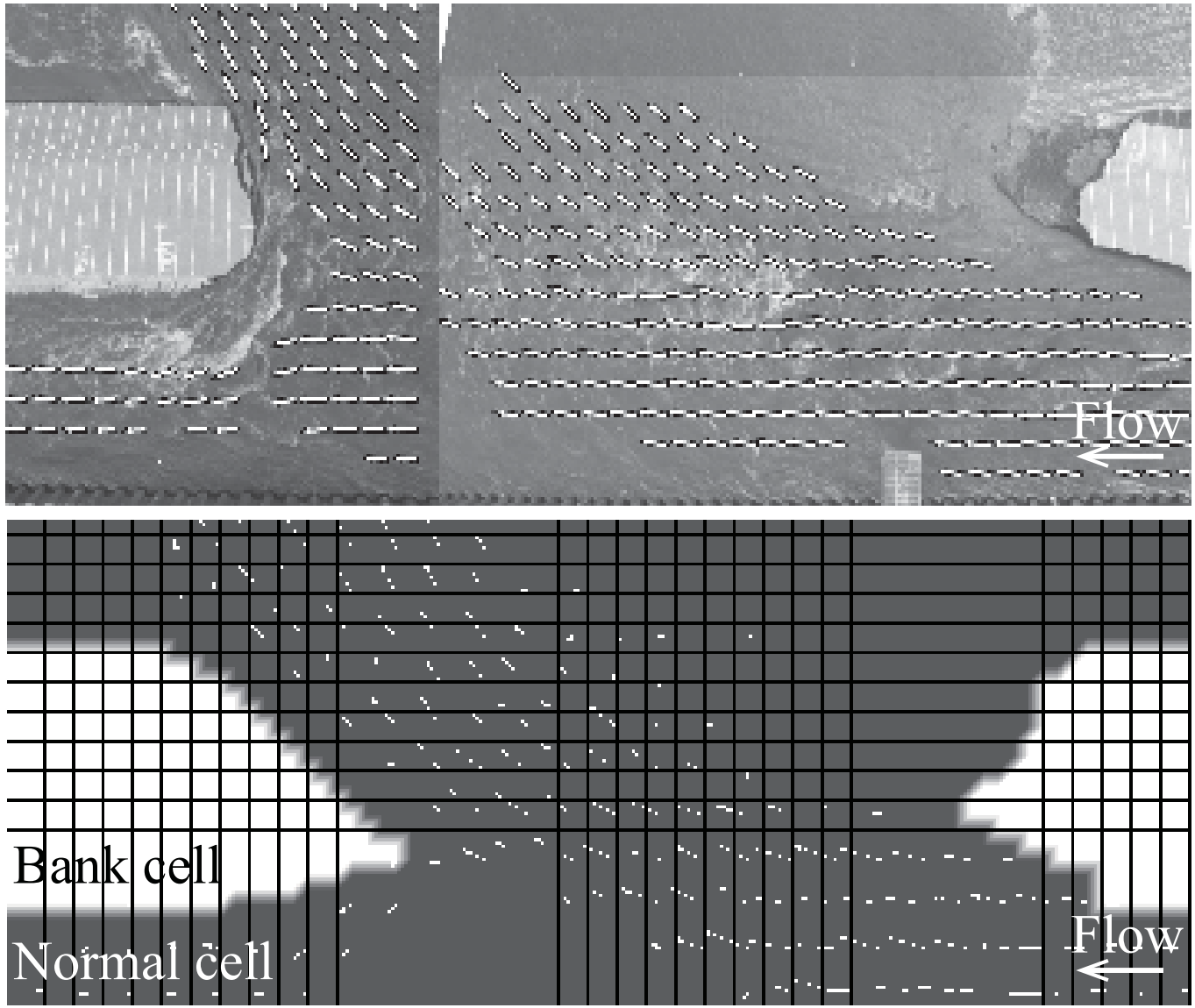

Levee breach widening width B ≒ 49 m

Legend for PIV flow rates ; → 5m/s

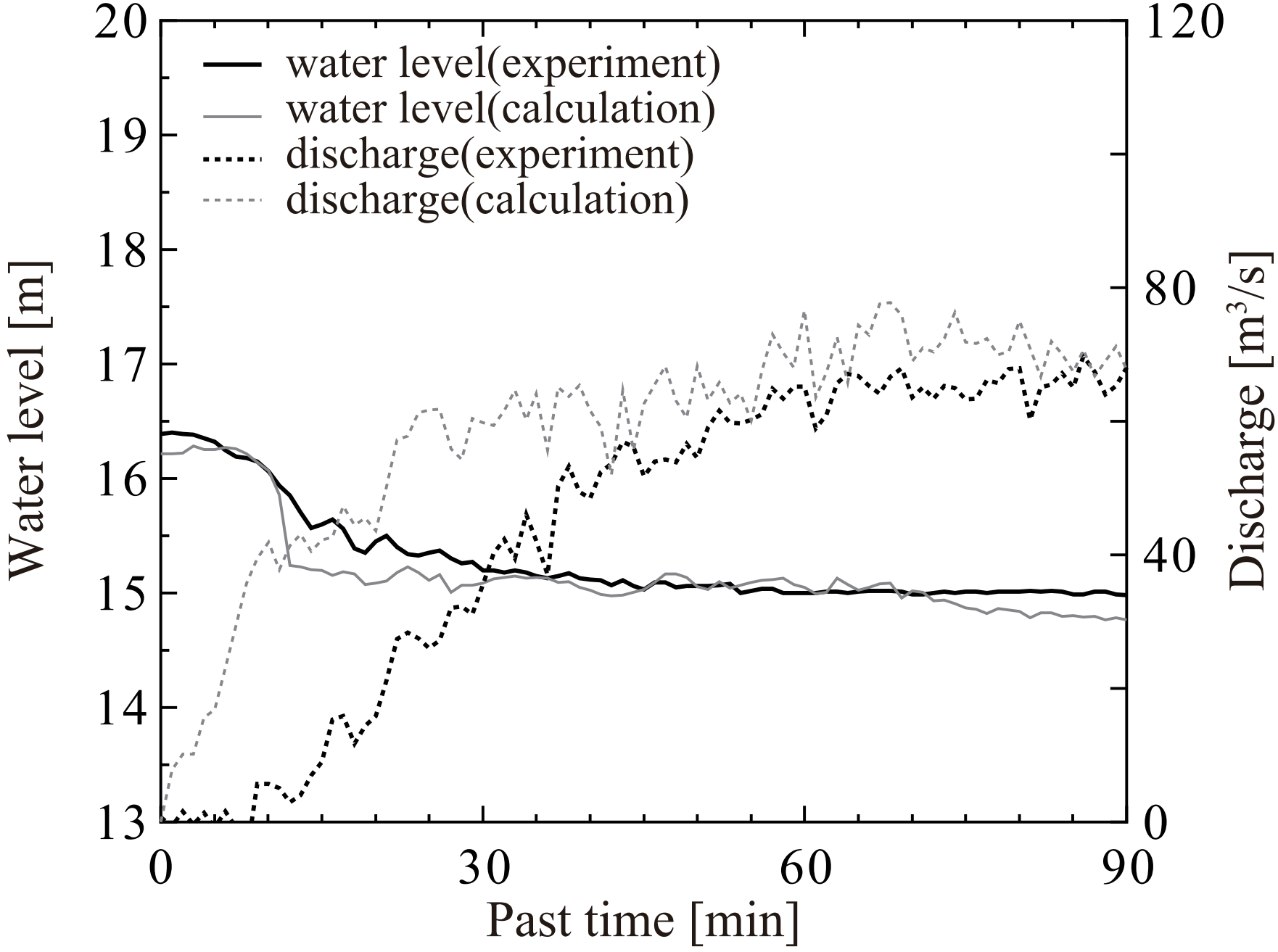
water level(experiment)
water level(calculation)
discharge(experiment)
discharge(calculation)
Water level [m]
Discharge [m3/s]
Past time [min]
20
19
18
17
16
15
14
13
120
80
40
0
0
30
60
90

Table 1. Test case condition

Case	Levee Material Size d_{50} (mm)	Crest Width (m)	Inflow Discharge (m^3/s)
1	5.4	3	70
2	4.9	3	35
3	0.2	3	70
4	0.7	6	70

Table 2. Calculation settings (conventional model).

Run	Maning's Roughness Coefficient	Material Size (mm)	Repose Angle (degrees)	Grid Size (m)
1	0.023	0.7	30	1×1
2	0.023	0.7	45	1×1
3	0.023	0.7	90	1×1
4	0.023	0.7	30	0.5×0.5

Table 3. Calculation settings (proposed model).

Run	Maning's Roughness Coefficient	Material Size (mm)	α	β
5	0.023	0.7	18	1.5
6	0.023	0.7	9	1.5
7	0.023	0.7	36	1.5
8	0.023	0.7	18	1.0
9	0.023	0.7	18	2.0